Earth and Planetary Science Letters 290 (2010) 142–149

Contents lists available at ScienceDirect

Earth and Planetary Science Letters

journal homepage: www.elsevier.com/locate/epsl

Diamondiferous kimberlites in central India synchronous with Deccan flood basalts

Bernd Lehmann [a,*], Ray Burgess [b], Dirk Frei [c], Boris Belyatsky [d], Datta Mainkar [e], Nittala V. Chalapathi Rao [a,f], Larry M. Heaman [g]

[a] Mineral Resources, Technical University of Clausthal, 38678 Clausthal-Zellerfeld, Germany
[b] School of Earth, Atmospheric and Environmental Sciences, University of Manchester, Manchester M13 9PL, UK
[c] Geological Survey of Denmark and Greenland (GEUS), 1359 Copenhagen, Denmark
[d] Precambrian Geology and Geochronology, Russian Academy of Sciences, Makarova emb. 2, 199034 St Petersburg, Russia
[e] Directorate of Geology and Mining, Ring Road 1, 492007 Raipur, Chhattisgarh, India
[f] Department of Geology, Banaras Hindu University, 221005 Varanasi, Uttar Pradesh, India
[g] Department of Earth and Atmospheric Sciences, University of Alberta, Edmonton, Canada T6G 2E3

ARTICLE INFO

Article history:
Received 9 September 2009
Received in revised form 1 December 2009
Accepted 4 December 2009
Available online 12 January 2010

Editor: R.W. Carlson

Keywords:
kimberlite
diamond
Deccan flood basalt
Behradih
Kodomali
India

ABSTRACT

Recently discovered diamondiferous kimberlite (Group-II) pipes in central India have surprisingly young $^{40}Ar/^{39}Ar$ whole rock and U–Pb perovskite ages around 65 million years. These ages overlap with the main phase of the Deccan flood basalt magmatism, and suggest a common tectonomagmatic control for both flood basalts and kimberlites. The occurrence of macrodiamonds in the pipes implies the presence of a thick subcratonic lithosphere at the Cretaceous/Tertiary boundary, significantly different from the present-day thickness of the Indian lithosphere. About one third of the Indian lithosphere was lost during or after the Deccan flood basalt event. The superfast northward motion of the Indian plate prior to the collision with Eurasia cannot be related to lithospheric thinning during the Gondwana break-up at 130 Ma, as previously thought.

1. Introduction

India is known for its historic diamonds from alluvial gravels. The source rocks for these diamonds are thought to be among the so far nearly 100 identified kimberlitic/lamproitic pipes and dikes which occur mostly in the Dharwar craton, southern India, and the Bundelkhand craton, central India, and which all have Mesoproterozoic ages with a peak at 1100 Ma (Kumar et al., 1993; Chalapathi Rao et al., 1999; Gregory et al., 2006) (Fig. 1). A cluster of several kimberlitic pipes has recently been discovered near Mainpur in the Bastar craton, central India, which yielded both macrodiamonds and microdiamonds (Newlay and Pashine, 1993; Chatterjee et al., 1995; Jha et al., 1995; Mainkar and Lehmann, 2007). We here demonstrate that these kimberlites are emplaced synchronous with the end-Cretaceous Deccan flood basalts.

The fact that the kimberlites carry macrodiamonds indicates the existence of a thick subcratonic lithospheric (non-convective) mantle in central India at the time of emplacement. Such a mantle root must reach below the 140 km depth needed to stabilize diamond from where explosive magmatism can bring diamonds to the Earth's surface sufficiently fast to partially survive phase transition and oxidation (Boyd and Gurney, 1986; Mitchell, 1986, 1995; Morgan, 1995). The thickness of the lithosphere at the time of the end-Cretaceous kimberlite volcanism in central India was significantly greater than the modern Indian lithosphere thickness of 80–100 km (Priestley and McKenzie, 2006; Kumar et al., 2007), and indicates substantial erosion and delamination of cratonic mantle lithosphere. This reorganization of lower cratonic lithosphere likely reflects the interaction of the Deccan mantle plume with concomitant flood basalt volcanism along the western Indian craton edge.

2. Geological setting, petrography and geochemistry

There are currently five kimberlite pipes known in the Mainpur kimberlite field which occur in a WNW-trending 15 by 3 km corridor within the metagranite–greenstone terrain of the easternmost Archean Bastar craton (Mainkar and Lehmann, 2007). The crystalline

* Corresponding author.
E-mail addresses: bernd.lehmann@tu-clausthal.de (B. Lehmann), ray.burgess@manchester.ac.uk (R. Burgess), df@geus.dk (D. Frei), bbelyatsky@mail.ru (B. Belyatsky), dmainkar@gmail.com (D. Mainkar), nvcr100@gmail.com (N.V.C. Rao), Larry.Heaman@ualberta.ca (L.M. Heaman).

0012-821X/$ – see front matter © 2009 Elsevier B.V. All rights reserved.
doi:10.1016/j.epsl.2009.12.014

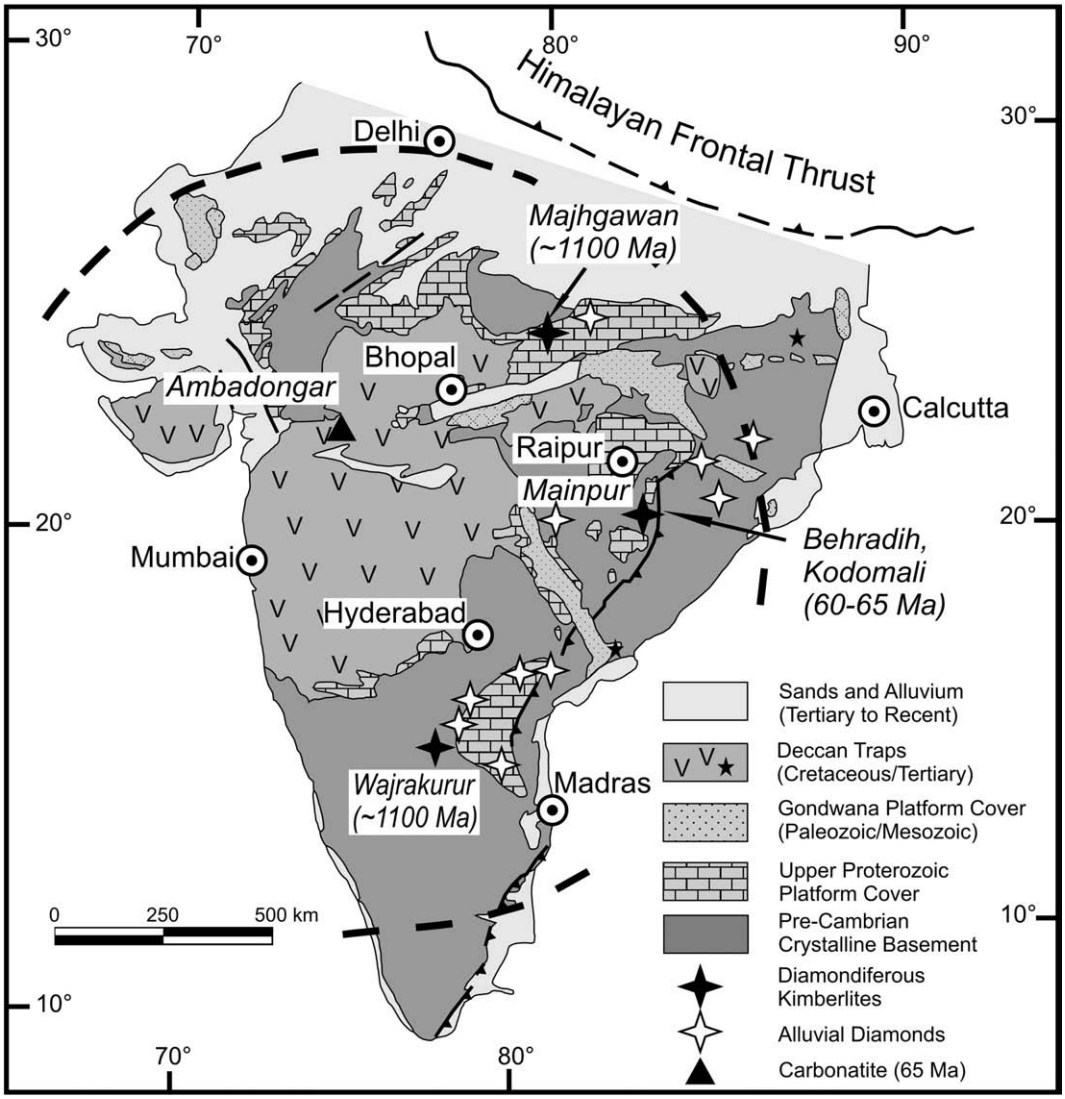

Fig. 1. Outline of the Deccan flood basalts and location of the three major diamondiferous kimberlite provinces in India (Wajrakurur and Majhgawan: 1100 Ma, Mainpur kimberlite field: 65 Ma), and Ambadongar carbonatite (65 Ma). The hypothetical Deccan mantle plume head (Cox, 1989) is shown in a thick stippled line. Note that erosional remnants of the Deccan Traps reach to the east coast (Rajahmundry Traps, 64.7 ± 0.5 Ma; Knight et al., 2003) and up to northeasternmost India (Salma dike, 65.4 ± 0.3 Ma; Kent et al., 2002), shown with an asterisk. Geological base map from Naqvi (2005).

basement is overlain by the platformal flat-lying and unmetamorphosed clastic sequence of the Neoproterozoic Pairi Group which is exposed in steep cliffs northeast of the kimberlite trend. Xenoliths of Pairi Group rocks occur in the pipes. The approximately circular Behradih pipe (200 m) and the NW elongated Kodomali pipe (200 × 80 m) are the largest kimberlite bodies in the Mainpur field. Behradih has yielded abundant macrodiamonds and was the site of illegal mining which recovered stones of up to 200 carats. Kodomali has yielded only microdiamonds so far. The area was explored by Oropa Ltd. until 2000 and is currently closed due to a legal dispute about ownership.

The Behradih pipe is hosted in coarse-grained biotite metagranite (Bundeli Granite) and both host-rock and kimberlite are affected by a pervasive propylitic overprint (chlorite–epidote–carbonate). The pipe is covered by a thick weathering blanket and has been explored by several drillholes down to about 200 m depth. The rock consists of diatreme-zone magmaclastic (pelletal lapilli) kimberlitic breccia (Mainkar and Lehmann, 2007). Subhedral to rounded macrocrysts of olivine (1–5 mm), pelletal lapilli (≤1 mm) and autoliths (several mm) are set in a very fine-grained glassy to yellow cryptocrystalline serpentine–chlorite matrix with abundant olivine microphenocrysts (<0.5 mm) and fine-grained phlogopite and clinopyroxene (Fig. 2). Phlogopite also occurs as macrocrysts, microphenocrysts and poikilitic aggregates in olivine. Rare, brownish-dark red pyrope xenocrysts (mostly calcic lherzolitic G9) are strongly resorbed, or occur as rounded inclusions in pelletal lapilli. Accessory phases are perovskite, spinel (magnesiochromite to chrome spinel), titanite, zircon, apatite and pyrite. Carbonate–talc–serpentine–chlorite alteration has strongly affected both the macrocryst/phenocryst phases and the groundmass. Xenoliths of feldspar-rich rock (dolerite and granite) as well as resorbed feldspar xenocrysts (plagioclase, microcline) are locally abundant. Silicate inclusions in diamond (mostly dodecahedral) have both eclogitic and peridotitic affinities. Infrared spectroscopy reveals variable nitrogen content and low nitrogen aggregation state (Jha et al., 1995).

The drillcore samples from Behradih have major and trace element concentrations within the range of kimberlite, but do not have the elevated K_2O, TiO_2 and P_2O_5 contents typical of lamproite (Mainkar

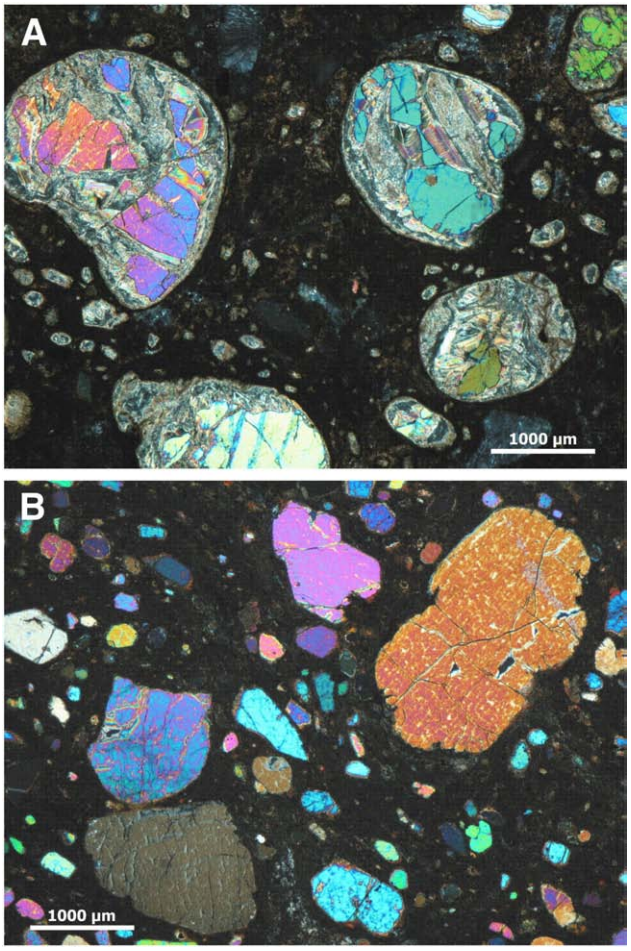

Fig. 2. Textural features of the Behradih and Kodomali kimberlites. A: Behradih: pelloidal-textured olivine macrocrystal kimberlite (DEB-3A/90; crossed nicols). B: Kodomali: olivine microcrysts in fine-grained clinopyroxene–phlogopite groundmass. (K-3; crossed nicols).

and Lehmann, 2007) (Table 1; Fig. 3). The samples display relatively elevated silica (40–43 wt.% SiO_2) and alumina contents (4–5 wt.% Al_2O_3), respectively, and relatively low magnesium contents (22–27 wt.% MgO; Fig. 3A and B). Some samples with Al_2O_3 contents of 5–6 wt.% contain petrographically identified K-feldspar xenocrysts, which also lead to elevated potassium contents of >2 wt.% K_2O for these contaminated samples. The titanium content of all samples is around 1 wt.% TiO_2. The CaO vs. Al_2O_3 variation plot (Fig. 3C) indicates that the Behradih samples are close to the compositional fields of South African Group-II kimberlites and olivine lamproites. The TiO_2 vs. K_2O plot (Fig. 3D) shows the distinct difference between the samples from the Behradih and Kodomali pipes compared to the Proterozoic Majhgawan pipe, the latter having elevated titanium content. The Behradih pipe depicts a large variation in potassium content, related to variable amounts of phlogopite, and the compositional field overlaps with the South African Group-I and Group-II kimberlite fields, but does not correspond to olivine lamproite. These features, as well as the diagnostic Nb–Zr plot of Fig. 4, identifies the Behradih samples as kimberlite, not lamproite. Their Sr and Nd isotope composition corresponds to African Group-II kimberlite (Table 2; Fig. 5).

The Kodomali pipe is emplaced in dolerite and is essentially unaffected by alteration. Fresh rock is exposed at the surface and has a distinctly inequigranular texture with macrocrysts (0.5–1 mm) and microphenocrysts of olivine and phlogopite set in a very fine-grained groundmass consisting of clinopyroxene, phlogopite and spinel microlites (Fig. 2). Serpentinization of olivine is minimal. Diopsidic clinopyroxene, present as acicular laths (<0.1 mm), is the typical groundmass phase. Phlogopite is mostly in the groundmass (<0.2 mm) and has a compositional range with 2–6 wt.% TiO_2 and 5–8 wt.% Al_2O_3, similar to South African Group-II kimberlite. Groundmass spinel ranges from Al–Mg to Ti–Mg chromite (Fareeduddin et al., 2006).

The chemical compositions of the Kodomali and Behradih kimberlites are similar, however Kodomali kimberlite has more elevated CaO contents; this can be accounted for mineralogically by the prominent calcic clinopyroxene component (Table 1). The Sr and Nd isotope compositions are also identical to Behradih, and correspond to African Group-II kimberlite, equivalent to orangeite of Mitchell (1995). The new data are within the broad Nd–Sr isotopic compositional trend of both Indian flood basalts and associated alkaline rocks, and is consistent with the involvement of an enriched continental lithospheric mantle source (Fig. 5).

3. $^{40}Ar/^{39}Ar$ geochronology

We analyzed three bulk-rock drillcore samples from the Behradih and two surface samples from the Kodomali kimberlite pipe by the $^{40}Ar/^{39}Ar$ step heating technique. In addition, we analyzed a granitic xenolith from Behradih drillcore. The $^{40}Ar/^{39}Ar$ analytical data are in ESM Table S1; plateau ages and statistics are summarized in Table 3; all ages are quoted with 2σ uncertainties. The results from $^{40}Ar/^{39}Ar$ dating are shown as apparent age and chemical (Ca/K and Cl/K) spectra in Fig. 6. Results from the Behradih pipe samples, shown in Fig. 6A, give congruent plateau ages of 65.4 ± 3.6 Ma (DEB 5/106 from 128 m drilling depth), 67.6 ± 1.7 Ma (DEB 5/114 from 174 m drilling depth), and 66.5 ± 1.0 Ma (DEB 4/56 from 91 m drilling depth). The latter sample consisted of very fine-grained matrix material only. The intercept on a $^{39}Ar/^{40}Ar$ vs. $^{36}Ar/^{40}Ar$ plot defines an initial $^{40}Ar/^{36}Ar$ of 309 ± 16, 299 ± 14, and 273 ± 14 for samples DEB5/106, DEB5/114, and DEB 4/56, respectively, consistent with the presence of atmospheric argon contamination in the samples. Based upon these $^{40}Ar/^{36}Ar$ ratios and the ^{36}Ar released, then atmospheric Ar typically accounted for between 15 and 40% of the ^{40}Ar released in the plateau steps (ESM Table S1). The weighted mean plateau age for the three samples is 66.7 ± 0.8 Ma. The age spectrum from the granitic xenolith DEB 1/26 is disturbed. The lowest temperature steps give increasing dates from a minimum of 70 Ma, most of the intermediate and high temperature steps give dates between 280 and 350 Ma, although there is a maximum date of 544 Ma in the middle section. The age spectrum of this granite xenolith attests to variable Ar resetting during heating and entrainment in the kimberlite pipe. The disturbed pattern also excludes the possibility of a hidden 65 Ma thermal source which could have completely reset the $^{40}Ar/^{39}Ar$ pattern in the kimberlite samples. Only a high temperature, or long duration, thermal event could have completely reset both the $^{40}Ar/^{39}Ar$ and U–Pb systems (see below), evidence for this is not supported by the lack of alteration or any re-crystallization textures in the kimberlite samples.

The two kimberlite samples from Kodomali give slightly younger plateau ages of 59.7 ± 2.1 Ma (K-4) and 64.0 ± 1.9 Ma (K-8) with a weighted mean plateau age of 62.1 ± 1.4 Ma (Fig. 6B). The intercepts on $^{39}Ar/^{40}Ar$ vs. $^{36}Ar/^{40}Ar$ plots define an initial $^{40}Ar/^{36}Ar$ of 303 ± 8 and 291 ± 21 for K-4 and K-8, respectively; consistent with atmospheric argon (ESM). Levels of atmospheric Ar contamination released in the plateau steps were similar to those obtained for the Behradih samples.

A previous attempt to date the Kodomali pipe (Chalapathi Rao et al., 2007) was hampered by the fact that a chloritized phlogopite megacryst was sampled. The resulting $^{40}Ar/^{39}Ar$ age spectrum had a large scatter, and the integrated age of 491 ± 11 Ma for 35% Ar release from 1000–1500 °C was erroneously interpreted as the kimberlite

Table 1
Representative chemical data for kimberlite samples from Behradih (20°12′52″N, 82°12′12″E; 570 m NN) and Kodomali (20°11′18″N, 82°14′30″E; 460 m NN).

		Behradih kimberlite, drill core						Kodomali kimberlite, surface			
		DEB-1/25	DEB-2/41	DEB-3A/90	DEB-4/58	DEB-5/105	DEB-5/116	Kod-3	Kod-4	K-7	K-8
wt.%											
SiO_2	XRF	41.14	40.24	40.29	40.97	42.89	42.16	42.96	43.06	43.12	42.89
TiO_2	XRF	1.13	0.97	1.29	1.05	1.11	1.08	1.25	1.24	1.26	1.29
Al_2O_3	XRF	4.80	4.57	4.79	4.48	5.17	4.58	5.25	5.36	5.22	5.21
ΣFe_2O_3	XRF	7.82	7.91	7.85	7.81	8.20	7.40	8.84	8.74	8.28	7.94
MnO	XRF	0.12	0.19	0.13	0.13	0.15	0.12	0.14	0.14	0.14	0.14
MgO	XRF	26.67	19.49	23.24	25.5	24.06	23.82	25.61	25.49	25.87	26.34
CaO	XRF	5.10	6.62	6.04	4.87	5.45	5.90	8.16	7.95	8.54	8.61
Na_2O	XRF	0.62	0.58	0.60	0.57	1.11	0.97	1.11	1.08	1.06	0.99
K_2O	XRF	1.96	2.00	3.02	2.04	2.55	2.78	1.71	2.01	1.72	2.11
P_2O_5	XRF	0.29	0.61	0.94	0.50	0.25	0.24	0.43	0.38	0.45	0.40
LOI	Grav	9.14	15.61	10.5	10.42	7.36	9.67	3.43	3.41	3.70	3.29
Sum		99.04	99.21	99.04	98.52	98.74	99.09	98.91	98.88	99.34	99.20
C.I.		1.6	2.1	1.7	1.7	1.8	1.8	1.7	1.7	1.8	1.7
Mg#		87.1	83.0	85.4	86.6	85.3	86.4	85.2	85.2	86.1	86.8
ppm											
Sr	XRF	781	609	1019	864	843	1003	982	948	1078	1052
Rb	XRF	143	86	154	179	166	134	87.9	90.4	81	90
Cu	XRF	30	28	37	31	45	34	71	69	46	44
Zn	XRF	65	58	66	73	66	63	65	69	46	48
Ni	XRF	1185	1076	1000	1253	1154	1088	1209	1178	884	906
Cr	XRF	1397	1140	1267	1160	1346	1256	1744	1763	1690	1690
Co	XRF	65	57	65	63	68	65	83	77	77	76
V	XRF	60	75	50	38	80	55	118	121	107	108
Sc	INA	10	10	12	12	13	11	17	15	16	16
Y	XRF	6	9	12	14	13	12	14.8	14.5	14	16
Zr	XRF	211	188	259	205	192	220	245	238	250	246
Nb	XRF	104	88	121	115	94	103	109	113	121	122
Ba	XRF	2241	1030	2350	6831	5316	1886	2773	2803	3898	3299
Ta	INAA	5.2	4.5	6.4	5.5	7.1	5.3	<5	<5	5	6
Pb	ICP	19	12	6	18	–	13	8	22	5	<5
Th	INA	13.2	14.1	17.5	21.3	19.2	15	18.4	18.2	17.9	18.3
U	INA	3.2	3.2	4.6	2.9	<0.5	2.9	3	3	3.2	3.3
Ga	XRF	6	5	9	7	7	7	8	6	7	8
La	INA	106	105	129	163	118	112	122	120	134	135
Ce	INA	149	151	191	238	234	165	213	210	216	212
Nd	INA	48	51	63	67	47	49	72	72	80	77
Yb	INA	0.9	0.8	1.0	1.6	1.7	1.0	1.0	1.0	1.0	0.9

emplacement age. The new $^{40}Ar/^{39}Ar$ data presented here were conducted at the same lab using the same analytical techniques, but with better sample control. We also analyzed a sample of a phlogopite megacryst from the Behradih pipe which gave a similarly scattered $^{40}Ar/^{39}Ar$ age spectrum with apparent age steps between 400 and 900 Ma (ESM). Apparent ages older than the kimberlite emplacement event are a commonly observed feature of mica megacrysts and phenocrysts in kimberlites. Their chronological significance is uncertain; they may be explained by the presence of excess ^{40}Ar inherited in the mantle that, due to the large grain size, was not completely outgassed during eruption to the surface (e.g., Kaneoka and Aoki, 1978; Phillips and Onstott, 1988; Phillips et al., 1999). Alternatively, it has been noted that some of the maximum apparent ages overlap with the timing of major cratonic tectonothermal events determined using other isotope chronometers, and this has led some authors to attribute the $^{40}Ar/^{39}Ar$ ages to mica growth during these events (e.g., Pearson et al., 1997; Hopp et al., 2008) with the suggestion that radiogenic ^{40}Ar may be retained above the conventional closure temperature of mica in a dry mantle environment (Kelley and Wartho, 2000; Wartho and Kelley, 2003).

4. U–Pb age determination on perovskite

A second independent age dating method was applied due to the locally pervasive alteration in the kimberlite pipes which may explain the relatively large scatter of the $^{40}Ar/^{39}Ar$ age data. We used laser-ablation magnetic-sectorfield inductively-coupled-plasma mass spectrometry (LA-SF-ICP-MS) on perovskite in bulk-rock polished sections (Frei et al., 2008; Hutchison and Frei, 2008; Frei and Gerdes, 2009; see ESM for data and analytical details). Perovskite occurs as an igneous groundmass mineral, commonly 10–50 μm in size, and analyses have been performed on three samples using 15 to 20 μm laser spot sizes. Between 17 and 23 individual spot analyses have been conducted for each of the three samples analyzed. Perovskite usually incorporates significant amounts of common Pb into its crystal lattice during crystallization (Heaman, 1989). Hence, U–Pb age dating of perovskite is associated with relatively large common Pb corrections. This is especially challenging for U–Pb age dating by laser-ablation ICP-MS techniques due to the interference of ^{204}Hg on ^{204}Pb caused by high Hg-backgrounds from the Ar plasma (e.g., Cox and Wilton, 2006). In this study the correction for common Pb was carried out according to the methods described by Frei and Gerdes (2009). The uncertainties associated with the common Pb correction are fully propagated into the quoted final age uncertainties. The low lead contents resulted in relatively large uncertainties associated with the common Pb correction. The weighted average common-lead corrected $^{206}Pb/^{238}U$ perovskite age determinations yielded precise and identical dates of 65.10 ± 0.80 and 65.09 ± 0.76 Ma (2σ) for two samples

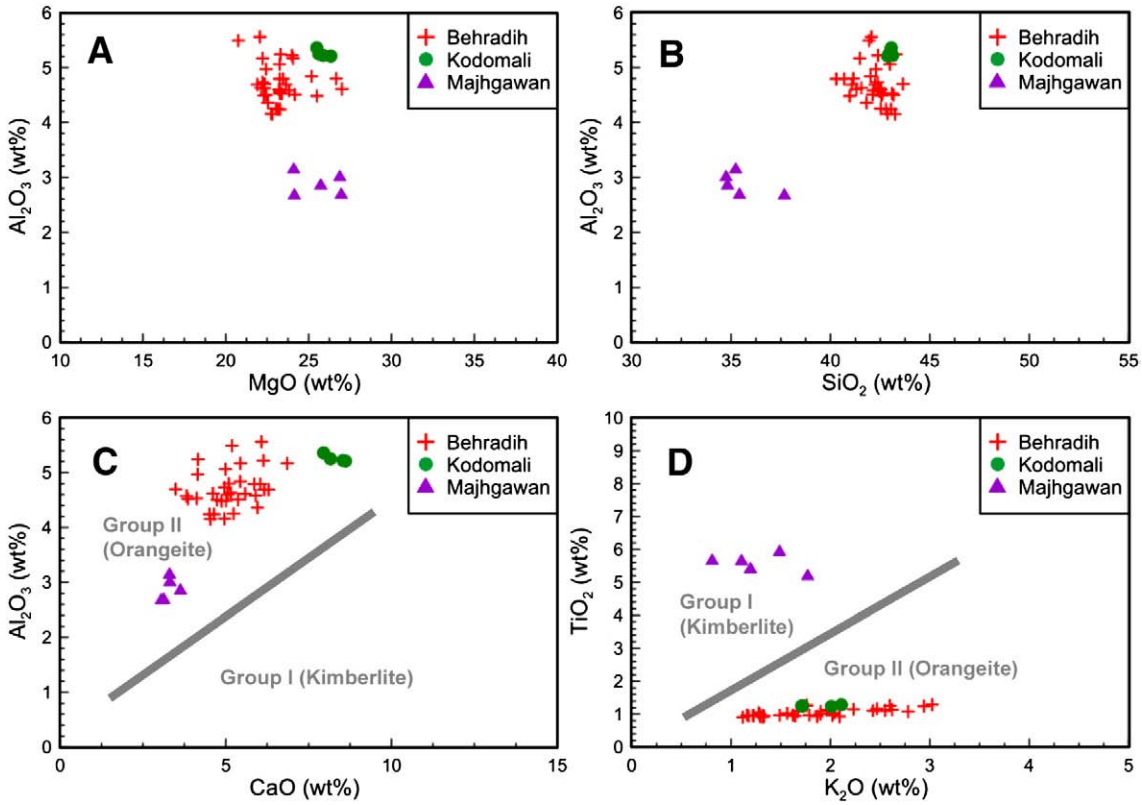

Fig. 3. Major-element plots for the Behradih and Kodomali kimberlite pipes (Mainpur kimberlite field) compared to the Majhgawan lamproite/kimberlite pipe. The Majhgawan pipe is the only currently mined primary diamond deposit in India, and has a much discussed chemical composition with features of both lamproite and kimberlite (Chalapathi Rao, 2005). Note that the two pipes from the Mainpur kimberlite field plot as Group-II kimberlite (orangeite) (reference data in Mitchell, 1995).
Data from Lehmann et al. (2006), Mainkar and Lehmann (2007).

from Behradih (DEB-1/25 and DEB 5/116 from 108 m and 184 m drilling depth, respectively) (ESM Fig. 4). The weighted average date for these two samples of 65.1 ± 0.4 Ma can be regarded as the best estimate for the emplacement age of the Behradih kimberlite. A sample from the Kodomali pipe (MKF-2c) gave a $^{206}Pb/^{238}U$ perovskite date of 62.3 ± 0.8 Ma, slightly younger than the Behradih age.

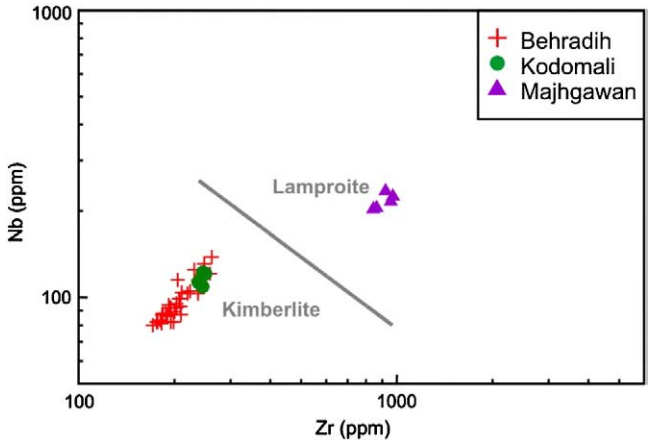

Fig. 4. Nb–Zr plot for the Behradih and Kodomali kimberlite pipes (Mainpur kimberlite field) compared to the Majhgawan pipe.
Data from Lehmann et al. (2006), Mainkar and Lehmann (2007).

5. Discussion and conclusions

The $^{40}Ar/^{39}Ar$ whole rock and U–Pb perovskite dates obtained in this study for two kimberlites from the Mainpur kimberlite field identify a previously unknown young end-Cretaceous/Paleocene kimberlite event in India. U–Pb perovskite dates of 65.1 ± 0.4 Ma and 62.3 ± 0.8 Ma were obtained for the diamond-bearing Behradih and Kodomali Group-II kimberlites and support the existence of a thick Indian lithosphere at this time. Although this age of kimberlite emplacement was previously unknown in India, it does coincide with kimberlite magmatism elsewhere including a number of pipes in the highly diamondiferous Lac de Gras field in NW Canada (Lockhart et al., 2004; Creaser et al., 2004; Heaman et al., 2004) and the youngest kimberlites in the Buffalo Head Hills field in northern Alberta, Canada (Eccles et al., 2008). In India the Mainpur kimberlite field formed synchronous with the Deccan flood basalt province, one of the largest igneous provinces on Earth, which was emplaced within a few million years around 65 Ma ago (Hofmann et al., 2000) (Fig. 7). The Deccan flood province comprises mainly basalts, but also melilitites, carbonatites, and lamprophyres. Diamondiferous kimberlites of all ages are largely restricted to thick and old (Archean) continental lithosphere (Clifford, 1966), and ancient, deep and non-convecting mantle is considered essential for the preservation of a long-lived diamond repository at the base of this cratonic mantle root (Helmstaedt and Gurney, 1995; Haggerty, 1999). The survival of Archean diamondiferous mantle roots requires relatively low temperatures, as expressed by fast shear wave velocities and low heat flow. Such relatively cool cratonic roots have been shown by seismic tomography to currently exist down to >300 km depth under the Baltic Shield, West Africa and central Siberia, while roots of >200 km exist in Canada, South Africa,

Table 2
Sr and Nd isotope data for samples from the Behradih and Kodomali pipes.

NN	Sample	Age	[Sm]	[Nd]	$^{147}Sm/^{144}Nd$	$^{143}Nd/^{144}Nd$	2s	ε	T(DM)	[Rb]	[Sr]	$^{87}Rb/^{86}Sr$	$^{87}Sr/^{86}Sr$	2s	$(^{87}Sr/^{86}Sr)t$
Behradih															
540	DEB 5/116	65	10.06	71.37	0.08500	0.512263	2	−6.39	1052	152.0	1062	0.41417	0.708690	7	0.708308
541	DEB 5/105	65	9.621	68.90	0.08400	0.512297	6	−5.72	1004	189.4	914.7	0.59903	0.708500	4	0.707947
542	DEB 4/58	65	11.68	84.82	0.08325	0.512315	5	−5.36	978	210.8	899.6	0.67800	0.708500	4	0.707874
543	DEB 3A/90	65	11.71	83.79	0.08450	0.512311	3	−5.45	992	169.8	1047	0.46911	0.708358	3	0.707924
544	DEB 2/41	65	8.988	59.14	0.09187	0.512098	6	−9.67	1317	95.92	645.3	0.43023	0.710623	4	0.710226
548	DEB 1/25	65	10.02	65.73	0.09215	0.512308	3	−5.57	1058	150.3	808.5	0.53788	0.708409	4	0.707913
Kodomali															
796	Kod-4	65	8.53	73.88	0.06980	0.512343	10	−4.70	857						
457	K-7	65	10.46	80.13	0.07894	0.512325	10	−5.13	935	80.67	1079	0.21631	0.707866	20	0.707666

western Australia, and northeastern South America (Artemieva and Mooney, 2001).

Diamonds may also originate from below the lithosphere as shown by the presence of certain mineral inclusions in diamond (e.g., majorite garnet) which indicate an ultradeep mantle origin for some diamonds (Haggerty, 1994; Stachel, 2001). However, independent of the ultimate origin of diamonds, their survival on rapid transport to Earth's surface will depend on the existence of a rigid (cool) mantle keel which reaches inside the diamond stability field (Morgan, 1995; Haggerty, 1999). Such a mantle keel with at least 140 km thickness was demonstrably available for the 65–62 Ma diamondiferous kimberlites in India. In contrast, the modern Indian lithosphere is only 80–100 km thick (Priestley and McKenzie, 2006; Kumar et al., 2007). Recent high-resolution *Ps* imaging in the Hyderabad area obtained a depth of only 65 km for the lithosphere–asthenosphere boundary in southern India (Rychert and Shearer, 2009). Thus at least one third of the thickness of cratonic root must have disappeared during the Tertiary. The age difference of about 3 Ma seen between the Behradih and Kodomali kimberlite pipes is statistically significant.

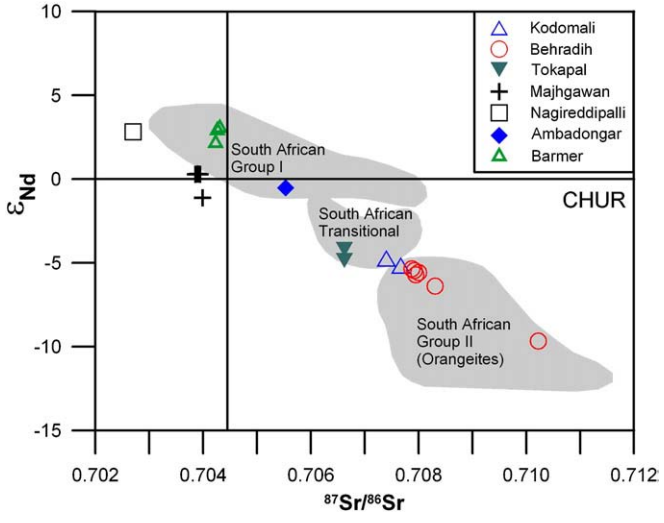

Fig. 5. Initial Sr versus initial Nd isotope composition of Indian kimberlites. Data on Kodomali and Behradih (65 Ma): this study; Tokapal (620 Ma) and Majhgawan (1100 Ma): Lehmann et al. (2006, 2007); Nagireddipalli (1100 Ma): Lehmann et al. (unpublished). Carbonatite data (Ambadongar and Barmer: 65 Ma) from Simonetti et al. (1998). The Sr–Nd composition of Deccan flood basalts covers all reference fields and extends over an even broader range (see data compilation in Mahoney et al., 2000). Reference fields for kimberlite groups (grey) based on data from Taylor et al. (1994), O'Brien and Tyni (1999), and Nowell et al. (2004).

Interestingly, both pipes have distinctly different diamond potentials. While Behradih samples have yielded many microdiamonds, as well as macrodiamonds, the Kodomali pipe has only yielded a small amount of microdiamonds. It may be that the slightly younger Kodomali pipe reflects an advanced degree of thermal erosion and delamination of the Indian cratonic root on impingement of the mantle plume which is thought to have produced the Deccan Traps. The extensive flood basalt volcanism of western India could be an expression of the lateral deflection of plume material towards the thinner craton margin while the plume head is characterized by much subdued small-degree melting and kimberlitic volcanism in central India (Foley, 2008).

Our data exclude major pre-Tertiary lithospheric thinning during the break-up of Gondwana which was proposed to explain the super-mobility of the Indian plate during the Cretaceous and Tertiary (Kumar et al., 2007). The exceptionally thin Indian lithosphere, compared to the thick lithosphere of its Gondwana paleo-neighbours of Australia, Antarctica and South Africa is apparently a relatively young feature which developed during or after the Deccan event.

Acknowledgements

We thank the Government of Chhattisgarh and the Directorate of Geology and Mining in Raipur for access to the drill core samples of this study. NVCR thanks the Alexander von Humboldt Foundation for a research fellowship in Clausthal. Graham Pearson, an anonymous referee, and the editor, Richard Carlson, provided helpful comments.

Appendix A. Supplementary data

Supplementary data associated with this article can be found, in the online version, at doi:10.1016/j.epsl.2009.12.014.

Table 3
Ar–Ar plateau ages and statistics.

Sample	Plateau age (Ma)	$\%^{39}Ar$	MSWD[a]	p[b]
DEB5/106	65.4 ± 3.6	98.1	0.69	0.71
DEB5/114	67.6 ± 1.7	85.1	1.3	0.27
DEB4/56	66.5 ± 1.0	72.5	0.11	1.00
K-4	59.7 ± 2.1	100	0.90	0.53
K-8	64.0 ± 1.9	85.8	1.5	0.13

[a] Mean square of weighted deviates.
[b] Probability of fit ($p \geq 0.05$).

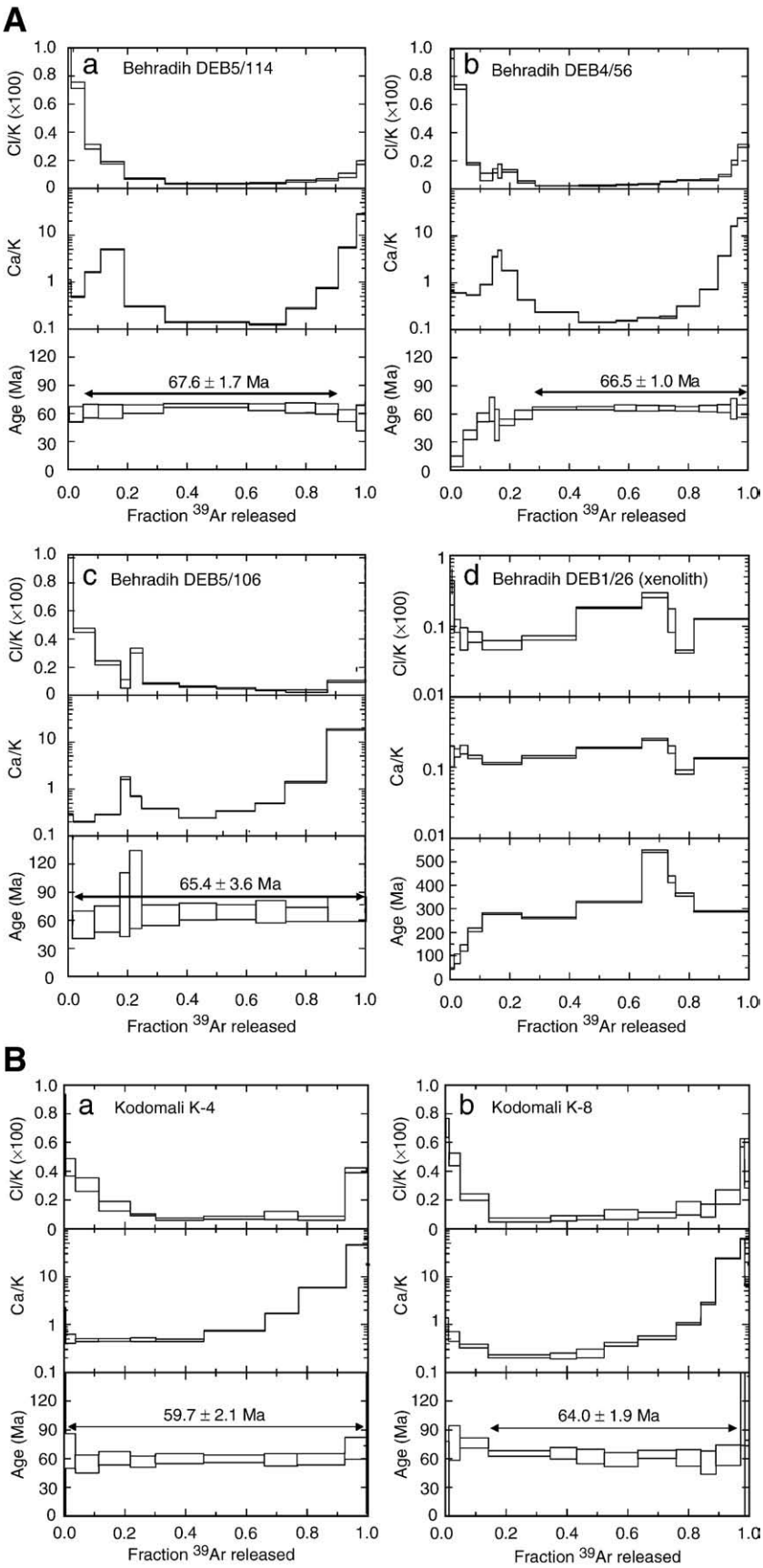

Fig. 6. $^{40}Ar/^{39}Ar$ whole rock age spectra of three kimberlite samples and one granitic xenolith from the Behradih pipe (A), and two kimberlite samples from the Kodomali pipe (B). All errors are 2σ. The analysis of bulk samples implies it is likely that Ar is released from several mineral phases during stepped heating. However, phlogopite is expected to be the most important K-bearing phase in kimberlites and the relatively constant and low Cl/K and Ca/K values occurring during intermediate temperature steps indicate release from this mineral. Argon released at lower temperatures appears to be from a component having high Cl/K, and at higher temperature the progressive increase in Ca/K is attributed to pyroxene. The Ar–Ar age pattern of a Behradih matrix sample has less scatter (c). $^{40}Ar/^{39}Ar$ age and chemical spectra for a granite xenolith in the Behradih kimberlite showing highly disturbed patterns (d).

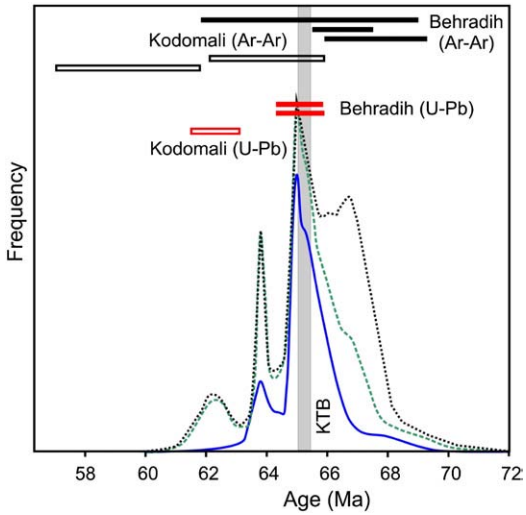

Fig. 7. Summary of $^{40}Ar/^{39}Ar$ whole rock ages and $^{238}U/^{207}Pb$ perovskite ages (2σ) for the Behradih and Kodomali kimberlite pipes, and frequency plot of $^{40}Ar/^{39}Ar$ ages for Deccan Trap flood basalts as compiled by Hofmann et al. (2000). The three curves represent the full data set of 33 samples (black solid line) and subsets of 24 (whole rock and mineral separates) and 13 (mineral separates) samples of top quality data. Each datum is given unit weight and represented by a Gaussian distribution with a standard deviation equal to the uncertainty in the age (Hofmann et al., 2000). Grey column marks the limits of the Cretaceous–Tertiary Boundary (KTB).

References

Artemieva, I.M., Mooney, W.D., 2001. Thermal structure and evolution of Precambrian lithosphere: a global study. J. Geophys. Res. 106, 16387–16414.

Boyd, F.R., Gurney, J.J., 1986. Diamonds and the African lithosphere. Science 232, 472–477.

Chalapathi Rao, N.V., 2005. A petrological and geochemical reappraisal of the Mesoproterozoic diamondiferous Majhgawan pipe of central India: evidence for transitional kimberlite–orangeite (group II kimberlite)–lamproite rock type. Mineral. Petrol. 84, 69–106.

Chalapathi Rao, N.V., Miller, J.A., Gibson, S.A., Pyle, D.M., Madhavan, V., 1999. Precise $^{40}Ar/^{39}Ar$ age determinations of the Kotakonda kimberlite and Chelima lamproite, India: implication to the timing of mafic dyke swarm emplacement in the eastern Dharwar Craton. J. Geol. Soc. India 53, 425–432.

Chalapathi Rao, N.V., Burgess, R., Anand, M., Mainkar, D., 2007. $^{40}Ar–^{39}Ar$ dating of the Kodomali Pipe, Bastar Craton, India: a Pan-African (491 ± 11 Ma) age of diamondiferous kimberlite emplacement. J. Geol. Soc. India 69, 539–546.

Chatterjee, B., Smith, C.B., Jha, N., Khan, M.W.Y., 1995. Kimberlites of Southeastern Raipur Kimberlitic Field, Raipur district, Madhya Pradesh, Central India. Ext. Abstr. 6th Intern. Kimberlite Conf, pp. 106–108. Novosibirsk.

Clifford, T.N., 1966. Tectono-metallogenic units and metallogenic provinces of Africa. Earth Planet. Sci. Lett. 1, 421–434.

Cox, K.G., 1989. The role of mantle plumes in the development of continental drainage patterns. Nature 342, 873–877.

Cox, R.A., Wilton, D.H., 2006. U–Pb dating of perovskite by LA-ICP-MS: an example from the Oka carbonatite, Quebec. Canada. Chem. Geol. 235, 21–32.

Creaser, R.A., Grutter, H., Carlson, J., Crawford, B., 2004. Macrocrystal phlogopite Rb–Sr dates for the Ekati property kimberlites, Slave Province, Northwest Territories, Canada. Lithos 76, 399–414.

Eccles, D.R., Creaser, R.A., Heaman, L.M., Ward, J., 2008. Rb–Sr and U–Pb geochronology and setting of the Buffalo Head Hills kimberlite field, northern Alberta. Can. J. Earth Sci. 45, 513–529.

Fareeduddin, Pant, N.C., Neogi, S., 2006. Petrology of the Kodomali diatreme, Mainpur area, Chhattisgarh, central India: implications for a Paleozoic orangeite field. J. Geol. Soc. India 68, 19–34.

Foley, S.F., 2008. Rejuvenation and erosion of the cratonic lithosphere. Nature Geosci. 1, 503–510.

Frei, D., Gerdes, A., 2009. Precise and accurate *in situ* U–Pb dating of zircon with high sample throughput by automated LA-SF-ICP-MS. Chem. Geol. 261, 261–270.

Frei, D., Hutchison, M.T., Gerdes, A., Heaman, L.M., 2008. Common-lead corrected U–Pb age dating of perovskite by laser ablation–magnetic sectorfield ICP-MS. Ext. Abstr. 9th Intern. Kimberlite Conf, vol. A-00216. 3 p.

Gregory, L.C., Meert, J.G., Pradhan, V., Pandit, M.K., Tamrat, E., Malone, S.J., 2006. A paleomagnetic and geochronologic study of the Majhgawan kimberlite, India: implications for the age of the Upper Vindhyan Supergroup. Precamb. Res. 149, 65–75.

Haggerty, S.E., 1994. Superkimberlites: a geodynamic window to the Earth's core. Earth Planet. Sci. Lett. 122, 57–69.

Haggerty, S.E., 1999. A diamond trilogy: superplumes, supercontinents, and supernovae. Science 285, 851–860.

Heaman, L.M., 1989. The nature of the subcontinental mantle from Sr–Nd–Pb isotopic studies on kimberlitic perovskite. Earth Planet. Sci. Lett. 92, 323–334.

Heaman, L.M., Kjarsgaard, B.A., Creaser; R.A., 2004. The temporal evolution of North American kimberlites. Lithos 76, 377–397.

Helmstaedt, H.H., Gurney, J.J., 1995. Geotectonic controls of primary diamond deposits: implications for area selection. J. Geochem. Explor. 53, 125–144.

Hofmann, C., Féraud, G., Courtillot, V., 2000. $^{40}Ar/^{39}Ar$ dating of mineral separates and whole rocks from the Western Ghats lava pile: further constraints on duration and age of the Deccan traps. Earth Planet. Sci. Lett. 180, 13–27.

Hopp, J., Trieloff, M., Brey, G.P., Woodland, A.B., Simon, N.S.C., Wijbrans, J.R., Siebel, W., Reitter, E., 2008. Ar-40/Ar-39-ages of phlogopite in mantle xenoliths from South African kimberlites: evidence for metasomatic mantle impregnation during the Kibaran orogenic cycle. Lithos 106, 351–364.

Hutchison, M.T., Frei, D., 2008. In-situ rock slab U–Pb dating of perovskite by laser ablation–magnetic sectorfield ICP-MS: a new tool for diamond exploration. Ext. Abstr. 9th Intern. Kimberlite Conf, vol. A-00223. 3p.

Jha, N., Smith, C.B., Griffin, B.J., Chatterjee, B., Pooley, G.D., 1995. Diamonds from kimberlites of Southeastern Raipur Kimberlitic Field, Raipur district, Madhya Pradesh, Central India. Ext. Abstr. 6th Intern. Kimberlite Conf, pp. 266–268. Novosibirsk.

Kaneoka, I., Aoki, K.-I., 1978. $^{40}Ar/^{39}Ar$ analyses of phlogopite nodules and phlogopite-bearing peridotites in South African kimberlites. Earth Planet. Sci. Lett. 40, 119–129.

Kelley, S.P., Wartho, J.A., 2000. Rapid kimberlite ascent and the significance of Ar–Ar ages in xenolith phlogopites. Science 289, 609–611.

Kent, R.W., Pringle, M.S., Müller, R.D., Saunders, A.D., Ghose, N.C., 2002. $^{40}Ar/^{39}Ar$ geochronology of the Rajmahal basalts, India, and their relationship to the Kerguelen Plateau. J. Petrol. 43, 1141–1153.

Knight, K.B., Renne, P.R., Halkett, A., White, N., 2003. $^{40}Ar/^{39}Ar$ dating of the Rajahmundry Traps, Eastern India, and their relationship to Deccan Traps. Earth Planet. Sci. Lett. 208, 85–99.

Kumar, A., Kumari, V.M.P., Dayal, A.M., Murthy, D.S.N., Gopalan, K., 1993. Rb–Sr ages of Proterozoic kimberlites of India: evidence for contemporaneous emplacement. Precamb. Res. 62, 227–237.

Kumar, P., Yuan, X.H., Kumar, M.R., Kind, R., Li, X.Q., Chadha, R.K., 2007. The rapid drift of the Indian tectonic plate. Nature 449, 894–897.

Lehmann, B., Mainkar, D., Belyatsky, B., 2006, The Tokapal crater-facies kimberlite system, Chhattisgarh, India: Reconnaissance petrography and geochemistry. J. Geol. Soc. India 68, 9–18.

Lehmann, B., Storey, C., Mainkar, D., Jeffries, T., 2007, In-situ U-Pb dating of titanite in the Tokapal-Bhejripadar kimberlite system, central India. J. Geol. Soc. India 69, 553–556.

Lockhart, G., Grutter, H., Carlson, J., 2004. Temporal, geomagnetic and related attributes of kimberlite magmatism at Ekati, Northwest Territories, Canada. Lithos 77, 665–682.

Mahoney, J.J., Sheth, H.C., Chandrasekharam, D., Peng, Z.X., 2000. Geochemistry of flood basalts of the Toranmal section, northern Deccan Traps, India: implications for regional Deccan stratigraphy. J. Petrol. 41, 1099–1120.

Mainkar, D., Lehmann, B., 2007. The diamondiferous Behradih kimberlite pipe, Mainpur Kimberlite Field, Chhattisgarh, India: reconnaissance petrography and geochemistry. J. Geol. Soc. India 69, 547–552.

Mitchell, R.H., 1986. Kimberlites: Mineralogy, Geochemistry and Petrology. Plenum Press, New York. London.

Mitchell, R.H., 1995. Kimberlites, Orangeites, and Related Rocks. Plenum Press, New York/London.

Morgan, P., 1995. Diamond exploration from the bottom up: regional geophysical signatures of lithosphere conditions favorable for diamond exploration. J. Geochem. Explor. 53, 145–165.

Naqvi, S.M., 2005. Geology and Evolution of the Indian Plate (from Hadean to Holocene 4 Ga to 4 Ka). Capital Publishers, New Delhi.

Newlay, S.K., Pashine, J., 1993. New find of diamond-bearing kimberlite in Raipur district, Madhya Pradesh, India. Current Science 65, 292–293.

Nowell, G.M., Pearson, D.G., Bell, D.R., Carlson, R.W., Smith, C.B., Kempton, P.D., Noble, S.R., 2004. Hf isotope systematics of kimberlites and their megacrysts: new constraints on their source regions. J. Petrol. 45, 1583–1612.

O'Brien, H.E., Tyni, M., 1999. Mineralogy and geochemistry of kimberlites and related rocks from Finland. Proc. 7th Intern. Kimberlite Conf, pp. 625–636.

Pearson, D.G., Kelley, S.P., Pokhilenko, N.P., Boyd, F.R., 1997. Laser $^{40}Ar/^{39}Ar$ dating of phlogopites from southern African and Siberian kimberlites and their xenoliths: constraints on eruption ages, melt degassing and mantle volatile compositions. Russian J. Geol. Geophys. 38, 106–117.

Phillips, D., Onstott, T.C., 1988. Argon isotopic zoning in mantle phlogopites. Geology 16, 542–546.

Phillips, D., Kiviets, G.B., Barton, E.S., Smith, C.B., Viljoen, K.S., Fourie, L.F., 1999. $^{40}Ar/^{39}Ar$ dating of kimberlites and related rocks: problems and solutions. In: Gurney, J.J., Gurney, J.L., Pascoe, M.D., Richardson, S.H. (Eds.), Proc. 7th Intern. Kimberlite Conf, vol. 2, pp. 391–396.

Priestley, K., McKenzie, D., 2006, The thermal structure of the lithosphere from shear wave velocities. Earth Planet. Sci. Lett. 244, 285–301.

Rychert, C.A., Shearer, P.M., 2009. A global view of the lithosphere–asthenosphere boundary. Science 324, 495–498.

Simonetti, A., Goldstein, S.L., Schmidberger, S.S., Viladkar, S.G., 1998. Geochemical and Nd, Pb, and Sr isotope data from Deccan alkaline complexes — inferences for mantle sources and plume–lithosphere interaction. J. Petrol. 39, 1847–1864.

Stachel, T., 2001. Diamonds from the asthenosphere and the transition zone. Eur. J. Mineral. 13, 883–892.

Taylor, W.R., Tompkins, L.A., Haggerty, S.E., 1994. Comparative geochemistry of West African kimberlites: evidence for a micaceous kimberlite endmember of sublithospheric origin. Geochim. Cosmochim. Acta 58, 4017–4037.

Wartho, J.A., Kelley, S.P., 2003. Ar-40/Ar-39 ages in mantle xenolith phlogopites: determining the ages of multiple lithospheric mantle events and diatreme ascent rates in southern Africa and Malaita, Solomon Islands. In: Vance, D., Muller, W., Villa, I.M. (Eds.), Geochronology: linking the isotopic record with petrology and textures: Geol. Soc. Spec. Publ., vol. 220, pp. 231–248.